Journal of Molecular Graphics and Modelling 72 (2017) 81–87

Contents lists available at ScienceDirect

Journal of Molecular Graphics and Modelling

journal homepage: www.elsevier.com/locate/JMGM

Topical Perspectives

Novel flavonol analogues as potential inhibitors of JMJD3 histone demethylase—A study based on molecular modelling

Sanchari Basu Mallik[a], Aravinda Pai[b], Rekha R. Shenoy[a], B.S. Jayashree[b,*]

[a] Department of Pharmacology, Manipal College of Pharmaceutical Sciences, Manipal University, Manipal, 576104, India
[b] Department of Pharmaceutical Chemistry, Manipal College of Pharmaceutical Sciences, Manipal University, Manipal, 576104, India

ARTICLE INFO

Article history:
Received 7 September 2016
Received in revised form 21 October 2016
Accepted 1 December 2016
Available online 13 December 2016

Keywords:
Epigenetics
JMJD3
Ligand docking
Natural flavonols
Myricetin

ABSTRACT

Epigenetic modulation of gene expression has drawn enormous attention among researchers globally in the present scenario. Since their discovery, Jmj-C histone demethylases were identified as useful markers in understanding the role of epigenetics in inflammatory conditions and in cancer as well. This has created arousal of interest in search of suitable candidates. Potential inhibitors from various other scaffolds such as hydroxyquinolines, hydroxamic acids and triazolopyridines have already been identified and reported. In this direction, our present study attempts to target one of the important members of the family-namely JMJD3 (also known as KDM6B), that plays a pivotal role in inflammatory and immune reactions. Using molecular modeling approaches, myricetin analogues were identified as promising inhibitors of JMJD3. Extensive literature review showed myricetin as the most promising flavonol inhibitor for this enzyme. It served as a prototype for our study and modification of it's scaffold led to generation of analogues. The ZINC database was used as a repository for natural compounds and their analogues. Using similarity search options, 65 analogues of myricetin were identified and screened against JMJD3 (PDB ID: 4ASK), using the high throughput virtual screening and ligand docking tools in Maestro Molecular Modeling platform (version 10.5) from Schrödinger, LLC. 8 analogues out of 65 were identified as the most appropriate candidates which gave the best pose in ligand docking. Their binding mode and energy calculations were analysed using induced fit docking (IFD) and prime-MMGBSA tool, respectively. Thus, our findings highlight the most promising analogues of myricetin with comparable binding affinity as well as binding energy than their counterparts that could be taken for further optimisation as inhibitors of JMJD3 in both *in vitro* and *in vivo* screening studies.

1. Introduction

The eukaryotic genome is unique and remains compressed in the form of chromatin. Histone proteins are the basic building blocks of chromatin, containing genomic DNA wrapped around them [1]. Regulation of gene expression is maintained by a dynamic balance between transcriptionally activating and repressive modifications on histone tails [2]. Methylation and demethylation of N-terminal tails of histones are two such post-translational modifications for epigenetic control of gene expression and are executed by histone lysine methyl transferases (KMTs) and histone lysine demethylases (HDMs) respectively [3]. Histone methylation can either lead to silencing or up-regulation of gene expression. For instance, methylation of H3K27 [4,5] and H3K9 [6] lead to silencing of genes. The histone demethylases responsible for these modulations are broadly classified as the lysine specific demethylases (LSD family) and the jumonji-C containing demethylases (Jmj-C family) [7].

Jmj-C demethylases belong to the 2-oxygenase class of enzymes, containing the Jumonji C catalytic domain. Similar to other known 2-oxygenases, Jmj-C enzymes utilize α-ketoglutarate and Fe^{+2} to catalyse the demethylation reaction [3]. The Jmj-C domain present in these enzymes contains a double-stranded-β-helical (DSBH) fold (also known as the *jelly roll*) that provides the rigid scaffold for α-ketoglutarate and Fe^{+2} [8]. Among the Jmj-C family members, UTX (KDM6A) and JMJD3 (KDM6B) are responsible for the removal of repressive methyl-marks on H3K27 histone [9,10]. At the catalytic site, the tri-methylated peptide of H3K27me3 binds to several amino acids and remains in close proximity with the Fe^{+2} moiety [11]. Like many other 2-oxygenases, the Jmj-C demethylases also contain the "facial triad" or the 2-His-1-carboxylate triad, consist-

* Corresponding author.
E-mail addresses: bs.jayashree@manipal.edu, jayashree.sy@gmail.com (B.S. Jayashree).

http://dx.doi.org/10.1016/j.jmgm.2016.12.002
1093-3263/

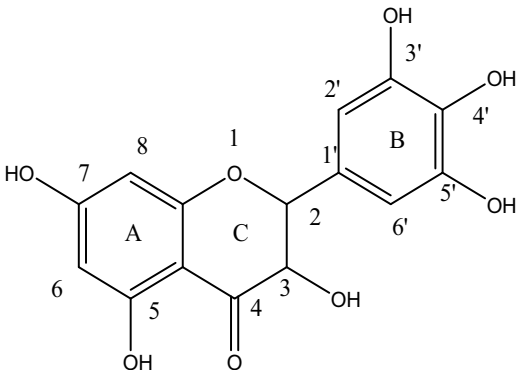

Fig. 1. Chemical structure of myricetin (ZINC03874317) for demonstrating the structural features of flavonols.

ing of three conserved residues bound to the catalytic iron [11–15]. The catalytic triad in JMJD3 consists of 2 histidines (H1390 and H1470) and a glutamate moiety (E1392) that facilitate the binding of α-ketoglutarate as a co-factor [11,12]. In spite of co-factor binding, the binding of the ligand to Fe^{+2} is equally important for enzyme activity [11].

Among these two enzymes, JMJD3 is inducible in nature and expressed only in response to inflammatory [10,16,17], viral [18] and oncogenic stimuli [19,20]. In macrophages stimulated by bacterial lipopolysaccharide (LPS), newly synthesized JMJD3 is responsible for the transcription of several genes including those for immune function as well as inflammatory reaction [21]. Recent discoveries emphasize that, JMJD3 levels are significantly increased in bone marrow isolates from human type-2 diabetic patients when compared to non-diabetic controls, probably leading to an exaggerated inflammatory process in affected individuals [22].

Epigenetic modifications pose as interesting therapeutic targets due to their reversible nature [23]. In this regard, several small molecule inhibitors of histone demethylases have been reported [3]. A recent review highlights that, some of the inhibitors of Jmj-C demethylases probably act as competitive inhibitors of α-ketoglutarate. However, alternative methods could be either competitive inhibition of histone substrates or inhibitors that target the non-catalytic domain of the enzyme [24]. Alternatively, a number of Jmj-C inhibitors have been developed that would chelate the Fe^{+2} ion to achieve enzyme inhibition [25]. Several such scaffolds have been identified to act against several Jmj-C family members from 2-hydroxyquinolines, hydroxamic acid derivatives and triazolopyridines classes [24].

Flavonoids are known as potent metal chelators and effective reactive oxygen species (ROS) scavenging agents. 3′ and 4′ -hydroxyl groups (in B ring) and 4-oxo and 5-OH groups (in C ring) of a flavone essentially participate in metal chelation (Fig. 1). The presence of these groups facilitates Fenton's reaction and leads to the generation of flavonoid-metal complexes [26,27]. In a high throughput screening of natural compound libraries, a large number of flavonoids and catechols were identified as non-competitive inhibitors of Jmj-C demethylases [28]. Other available literature, also supports naturally occurring flavonols as inhibitors of Jmj-C family of histone demethylases [3].

Previous scientific reports state that inflammatory stimuli such as bacterial lipopolysaccharide (LPS) specifically upregulates the expression of JMJD3 among all other Jmj-C genes in murine macrophage cell lines [10]. Myricetin, a known non-specific inhibitor of Jmj-C enzymes, has been shown to modulate the activation of mouse bone marrow derived dendritic cells in presence of LPS, by modulating the release of TNF-α, IL-6 and IL-12 via down-regulation of NF-κB binding [29,30]. In RAW 264.7 cells (murine macrophages), it significantly inhibits the production of TNF-α and IL-1β, thereby controlling the inflammatory reaction [30,31]. Therefore, based on the proven reports, we hypothesize that, myricetin could inhibit JMJD3. According to this hypothesis, we have undertaken the ligand docking simulation study on the myricetin-analogues for their binding affinity and potential of inhibiting JMJD3.

2. Materials and methods

Molecular docking studies on myricetin and it's analogues were performed using Maestro Moelcular Modeling platform (version 10.5) by Schrödinger, LLC [32]. The atomic co-ordinates of human JMJD3 (KDM6B) histone demethylase enzyme were downloaded from the Protein Data Bank [33,34] using PDBID 4ASK [11]. The Fe^{+2} moiety present in JMJD3 is represented by Co^{+2} in 4ASK. 65 analogues of myricetin were identified using a similarity search on ZINC database [35,36] and further screened for their binding affinity to JMJD3.

2.1. Ligand preparation

LigPrep tool was used for ligand optimization which produced lowest energy 3D structures with corrected chiralities [37]. The process was performed at neutral pH and under OPLS 2005 force field [38].

2.2. Protein preparation and grid generation

The biological unit of the protein was subjected for protein preparation prior to docking [39,40]. During protein preparation, missing side chains of the proteins were filled using the Prime tool [41] and missing residues were updated. The protein was further refined using restrained optimization, by removal of heavy atoms and water molecules. After protein preparation, receptor grid was generated keeping the van der Waals scaling factor as 1.00 and charge cut off of 0.25 subjected to OPLS 2005 force field [38]. A cubic box of specific dimensions centred around the centroid of the active site was generated for each protein.

2.3. Ligand docking

The analogues were first screened using high throughput virtual screening (HTVS) method and re-analysed using standard precision (SP) and extra-precision (XP) [42] flexible ligand docking in Glide [43,44]. van der Waals scaling factor and partial charge cut off was selected to be 0.80 and 0.15, respectively for ligand atoms. The optimized ligands were utilized for this purpose. The bound ligand was selected for root mean square deviation (RMSD) calculations. The best docked pose with lowest Glide score value was recorded for each ligand. The top analogues which showed docking scores more than −9.0 kcal/mol, were further chosen for induced fit docking (IFD) and ADME screening.

2.4. Induced fit docking (IFD) Standard precision (SP)

IFD-SP function was performed on the 8 identified compounds and myricetin, based on their binding scores in extra precision glide docking (XP) [45]. Under the IFD-SP protocol, the enzyme was optimized further and a grid was generated by choosing the bound ligand. Side chains of the enzyme were trimmed automatically based on B-factor and the protein was further prepared under constrained refinement using receptor and ligand van der Waal's scaling of 0.5 each. A maximum of 20 poses were generated for each ligand. Prime refinement was carried out for residues within 5 Å of the ligand. Glide re-docking was carried out for structures within

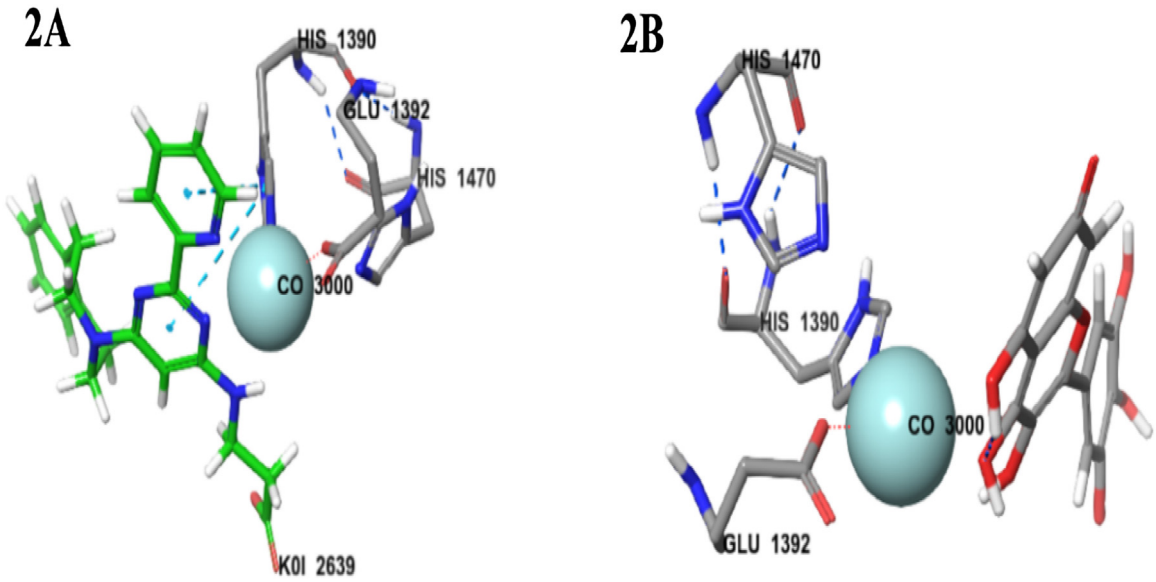

Fig. 2. Figure depicting the interactions of (A) GSK-J1 (in green) and (B) Myricetin (in grey) with the facial triad of JMJD3; HIS = Histidine, GLU = Glutamate. (For interpretation of the references to colour in this figure legend, the reader is referred to the web version of this article.)

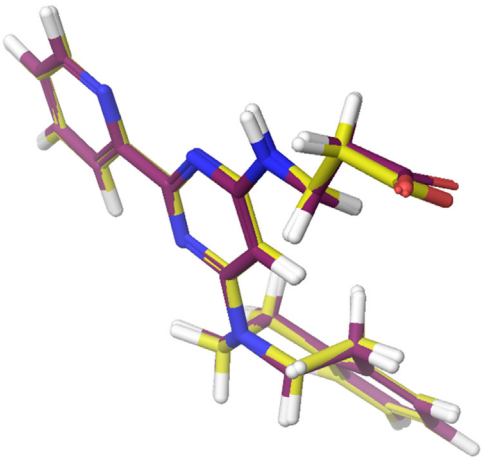

Fig. 3. Figure depicting superposition of bound GSKJ1 (separated from PDB 4ASK) and docked pose of GSKJ1 in extra precision docking for root mean square deviation (RMSD) calculation (RMSD = 0.135).

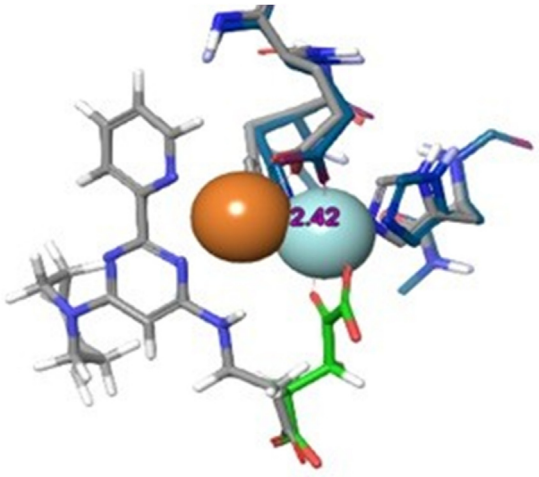

Fig. 4. Figure depicting binding of alpha ketoglutarate (green) to the catalytic site and the shift in catalytic iron [overlapping structures of PDBs 2XUE (iron in blue) and 4ASK (iron in orange) facial triad] caused by the attachment of GSK-J1 (grey and blue). (For interpretation of the references to colour in this figure legend, the reader is referred to the web version of this article.)

30 kcal/mol of the best structure and within the top 20 structures overall. IFD score for each of these compounds was generated and reported, which is calculated as:

$$\text{IFDScore} = 1.0 * \text{Prime\_Energy} + 9.057 * \text{GlideScore} + 1.428 * \text{Glide\_Ecoul}$$

2.5. Free energy calculations

The free energies of the enzyme-ligand complex of the identified myricetin analogues from ZINC database were estimated using MM-GBSA method, implemented in Prime module of the Schrodinger's molecular modeling platform. Prime utilizes the VSGB 2.0 solvation model [47] and the OPLS2005 force field [38] to simulate these interactions.

2.6. ADME analysis

The ADME characteristics of all selected compounds were predicted using QikProp module, in order to obtain an understanding of solubility and absorption levels of the compounds [48]. Descriptors like QPlogPo/w, QPlogS, QPPCaco, rule of 5 and % human oral absorption were calculated using this module.

3. Results

3.1. Molecular modeling

The binding site of JMJD3 consists of the central catalytic iron (Fe^{+2}) and three conserved amino acid residues Histidine 1470, Histidine 1390 and Glutamate 1392 forming the "facial triad". The co-factor alpha-ketoglutarate interacts with two of these residues,

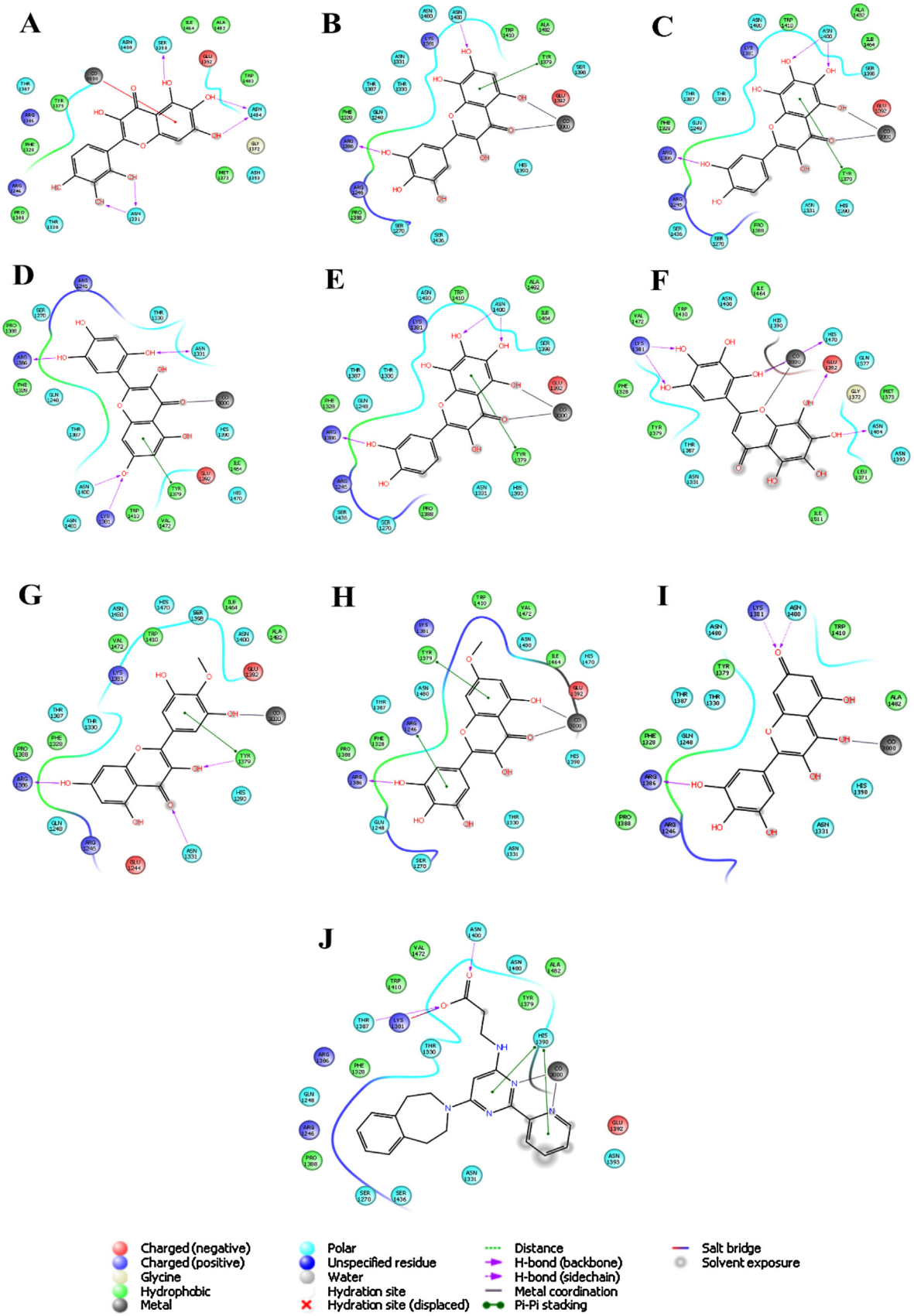

Fig. 5. Ligand interaction diagrams for top scoring ligands (A) ZINC15271426; (B) ZINC15271652; (C) ZINC15271738; (D) ZINC14436469; (E) ZINC14436799; (F) ZINC14616644; (G) ZINC13838618; (H) ZINC13838621; (I) ZINC03874317; (J) GSK-J1.

Table 1
Summary of SP and XP docking scores, XP H bond, IFD score and dG binding for the 8 identified ligands, myricetin (ZINC03874317) and GSKJ1.

SL. No.	ZINC ID	Dock score[a] (SP)	XP G Score[a]	XP H bond[a]	IFD Score[a]	dG bind[a] (MMGBSA)
1	ZINC14436469	−7.455	−9.911	−4.231	−955.887	−40.946
2	ZINC03874317	−8.756	−9.497	−3.478	−957.447	−44.078
3	ZINC15271652	−6.924	−9.261	−2.129	−959.367	−44.033
4	ZINC14616644	−7.223	−9.204	−2.812	−961.646	−42.966
5	ZINC14436799	−6.648	−9.167	−3.937	−957.991	−34.153
6	ZINC15271426	−9.126	−9.138	−3.089	−958.964	−41.271
7	ZINC13838621	−9.093	−9.118	−5.036	−958.374	−52.573
8	ZINC15271738	−6.869	−9.086	−3.143	−959.485	−39.706
9	ZINC13838618	−6.554	−9.069	−3.29	−957.623	−43.321
10	GSK-J1	−9.370	−9.370	−2.129	−970.341	−12.259

[a] All values are expressed as kcal/mol.

Table 2
Summary of key interacting protein residues at the catalytic site of JMJD3 for 8 identified ligands, myricetin (ZINC03874317) and GSKJ1.

SL.No.	ZINC ID	Key interacting residues
1	ZINC14436469	TYR1379, SER1436,
2	ZINC03874317	ARG1246, SER1436, LYS1381, ASN1400
3	ZINC15271652	ARG1386, ASN1331, TYR1379, LYS1381,
4	ZINC14616644	ASN1400, LYS1381, TYR1379, ARG1386, ASN1331
5	ZINC14436799	TYR1379, ASN1400, LYS1381, ASN1331, ARG1386
6	ZINC15271426	TYR1379, ASN1400, SER1436
7	ZINC13838621	ASN1331, THR1387, HIS1390, ASN1480, LEU1371, SER1398, ASN1393
8	ZINC15271738	TYR1379, THR1387, ARG1246, SER1346, ASN1400,
9	ZINC13838618	ASN1331, ARG1386, ASN1400
10	GSK-J1	HIS1390, ASN1400, LYS1381

TYR—Tyrosine; SER—Serine; ARG—Arginine; LYS—Lysine; ASN—Asparagine; THR—Threonine, HIS—Histidine; LEU—Leucine.

which are critical for catalytic activity of the enzyme[12]. The PDB file used for the present study contains the co-crystal structure of JMJD3 and its selective inhibitor GSK-J1 and therefore, root mean square deviation (RMSD) value was used for internal validation of the docking process. RMSD values obtained for each docking protocol was well within the acceptable limit (less than 2.0) as demonstrated in Fig. 3 by superposition of the bound and docked ligand GSK-J1.

3.1.1. Ligand docking

ZINC database search was performed and based on that, 65 analogues of myricetin were identified. High throughput virtual screening, standard precision and extra precision ligand docking were carried out on the 65 identified myricetin (ZINC3874317) analogues. We were able to identify 8 (ZINC15271426; ZINC15271652; ZINC15271738; ZINC14436469; ZINC14436799; ZINC14616644; ZINC13838618; ZINC13838621) of these 65 analogues which had binding affinities above 9.0 kcal/mol. All analogues showed interactions with the catalytic triad amino acids as well as with other residues important for enzyme inhibition. In all the chosen ligands, the 4-oxo group along with the 3 and 5-hydroxyl groups participated in metal co-ordination bonds with the Co^{+2} atom as demonstrated in Fig. 5. The position of these analogues in the catalytic pocket seems to be blocking the free binding sites on the Co^{+2} atom, but does not seem to hinder with α-ketoglutarate binding. Unlike our ligands, GSK-J1 is known to competitively bind to the catalytic iron and cause a shift in the metal atom of 2.42 Å (as demonstrated in Fig. 4). Our findings are in accordance with those reported by Kruidenier et al. [11]. A 3D image of binding of GSKJ1 (Fig. 2A) and myricetin (Fig. 2B) have been incorporated for ease of understanding.

3.1.2. Induced fit docking- Standard precision (IFD-SP)

The IFD-SP protocol allows flexibility of the protein residues at the binding site, which often complicates ligand binding in reality. IFD was carried out for the 8 identified compounds from top XP G scores along with myricetin. From IFD, the key protein residues at the catalytic site which interacted with the ligands were identified and are summarised in Table 2. Additionally, IFD scores were identified for each ligand and are summarized in Table 1.

3.1.3. Ligand interaction

Ligand interactions were observed from both XP ligand docking and further analysed from IFD-SP protocol. All ligands, except ZINC15271426, ZINC14616644 and ZINC03874317 (myricetin), showed pi-pi stacking interaction with tyrosine residue (TYR1379) (Fig. 5). Additional binding to serine residue (SER1246) which is important for specificity was observed in ligands ZINC3874317 (myricetin) and ZINC15271738 (Fig. 5). Due to the presence of multiple hydroxyl groups, the ligands showed participation in hydrogen bonding with multiple residues. The residues interacting with each ligand, as seen in the IFD-SP protocol have been summarized in Table 2.

3.1.4. Free energy calculations

The molecular mechanics/generalised born and surface area (MM/GBSA) method is one of the popular methods used for estimation of the free energy of the binding of small ligands to biological macromolecules and is based on the molecular dynamics simulations of the receptor-ligand complex. The Prime MMGBSA approach determines the free energy of binding of the ligand-receptor complex [46]. Free energy calculations were carried out on all identified analogues. In this study, the analogues showed binding energies (dG bind; Table 1) comparable to that of myricetin (ZINC03874317). However, the identified ligands showed more negative dG bind values than that of the inhibitor GSKJ1, suggesting stronger binding and the formation of more stable ligand-protein complexes (Table 1).

3.1.5. ADME profile analysis

The ADME profile analysis of the selected compounds was carried out using Qikprop module [48]. Different cut-off values were pre-assigned for the parameters estimated, in order to categorize the compounds. The ADME properties of the selected molecules are

Table 3
Summary of ADME profiles for the 8 identified analogues and myricetin (ZINC03874317).

Sl. No.	ZINCID	Molecular weight	QPlogPo/w[a]	QPlogS[b]	QPPCaco[c]	Rule of 5[d]	% Human oral asorption[e]
1	ZINC14436469	318.239	−0.235	−2.442	9.748	1	30.31
2	ZINC03874317	318.239	−0.747	−2.257	8.538	1	26.281
3	ZINC15271652	334.239	−0.867	−2.211	3.69	1	19.058
4	ZINC14616644	350.238	−1.446	−2.058	1.511	1	8.731
5	ZINC14436799	318.239	−0.223	−2.485	9.412	1	30.106
6	ZINC15271426	334.239	−0.792	−2.069	5.638	1	22.792
7	ZINC13838621	332.266	0.53	−2.922	26.616	0	55.557
8	ZINC15271738	334.239	−0.816	−2.226	4.237	1	20.434
9	ZINC13838618	332.266	0.582	−2.943	27.826	0	56.205
10	ZINC06525297	318.239	−0.711	−2.12	10.511	1	28.107

[a] Predicted octanol/water partition co-efficient logP (acceptable range from −2 to 6.5).
[b] Predicted aqueous solubility logS (acceptable range from −6.5 to 0.5).
[c] Predicted Caco-2 cell permeability in nm/s (acceptable range: <25 is poor and >500 indicates high permeability).
[d] Number of violations of Lipinski's rule of five (maximum 4).
[e] Percentage human oral absorption (<25% is poor and >80% is high).

summarized in Table 3. All compounds showed ADME characteristics within acceptable range including very little or no deviation from Lipinski's rule of five. The compounds did not show substantial human oral absorption profiles as flavonols are reported to show poor oral absorption and low oral bioavailability.

4. Conclusions

Flavonols are known for their diverse pharmacological properties. Epigenetic modulation is one of the areas of research interest in the present scenario. Our study, emphasized on understanding the epigenetic modulation by myricetin and its analogues, mediated through JMJD3 inhibition, using molecular docking approach. This study, thus led to the identification of 8 successful candidates out of 65 compounds screened with binding affinity above −9.0 kcal/mol. Further, *in vitro* and *in vivo* studies may be crucial to understand the interactions of these ligands from an enzyme inhibition point of view.

Funding source

This research work was supported by Department of Science and Technology, Government of India, through the award of INSPIRE Fellowship to Sanchari Basu Mallik (IF150659).

Conflict of interest

The authors declare that there is no conflict of interest.

Acknowledgements

The authors would like to thank the Department of Science and Technology, Government of India, for their kind support. The authors would also like to acknowledge the facilities provided by Manipal College of Pharmaceutical Sciences and Manipal University, instrumental in executing this research work.

Appendix A. Supplementary data

Supplementary data associated with this article can be found, in the online version, at http://dx.doi.org/10.1016/j.jmgm.2016.12.002.

References

[1] P. Cheung, P. Lau, Epigenetic regulation by histone methylation and histone variants, Mol. Endocrinol. 19 (2005) 563–573.
[2] K.M. Arcipowski, C.A. Martinez, P. Ntziachristos, Histone demethylases in physiology and cancer: a tale of two enzymes, JMJD3 and UTX, Curr. Opin. Genet. Dev. 36 (2016) 59–67.
[3] B. Lohse, J.L. Kristensen, L.H. Kristensen, K. Agger, K. Helin, M. Gajhede, et al., Inhibitors of histone demethylases, Bioorg. Med. Chem. 19 (2011) 3625–3636.
[4] R. Cao, L. Wang, H. Wang, L. Xia, H. Erdjument-Bromage, P. Tempst, et al., Role of histone H3 lysine 27 methylation in Polycomb-group silencing, Science 298 (2002) 1039–1043.
[5] J. Müller, C.M. Hart, N.J. Francis, M.L. Vargas, A. Sengupta, B. Wild, et al., Histone methyltransferase activity of a Drosophila Polycomb group repressor complex, Cell 111 (2002) 197–208.
[6] A.H. Peters, J.E. Mermoud, D. O'Carroll, M. Pagani, D. Schweizer, N. Brockdorff, et al., Histone H3 lysine 9 methylation is an epigenetic imprint of facultative heterochromatin, Nat. Genet. 30 (2002) 77–80.
[7] S.M. Westaway, A.G. Preston, M.D. Barker, F. Brown, J.A. Brown, M. Campbell, et al., Cell penetrant inhibitors of the KDM4 and KDM5 families of histone lysine demethylases. 1. 3-Amino-4-pyridine carboxylate derivatives, J. Med. Chem. 59 (2016) 1357–1369.
[8] C. Johansson, A. Tumber, K. Che, P. Cain, R. Nowak, C. Gileadi, et al., The roles of Jumonji-type oxygenases in human disease, Epigenomics 6 (1) (2014).
[9] S. Hong, Y.-W. Cho, L.-R. Yu, H. Yu, T.D. Veenstra, K. Ge, Identification of JmjC domain-containing UTX and JMJD3 as histone H3 lysine 27 demethylases, Proc. Natl. Acad. Sci. 104 (2007) 18439–18444.
[10] F. De Santa, M.G. Totaro, E. Prosperini, S. Notarbartolo, G. Testa, G. Natoli, The histone H3 lysine-27 demethylase Jmjd3 links inflammation to inhibition of polycomb-mediated gene silencing, Cell 130 (2007) 1083–1094.
[11] L. Kruidenier, C.-w. Chung, Z. Cheng, J. Liddle, K. Che, G. Joberty, et al., A selective jumonji H3K27 demethylase inhibitor modulates the proinflammatory macrophage response, Nature 488 (2012) 404–408.
[12] J.W. Højfeldt, K. Agger, K. Helin, Histone lysine demethylases as targets for anticancer therapy, Nat. Rev. Drug Discov. 12 (2013) 917–930.
[13] K.D. Koehntop, J.P. Emerson, L. Que Jr., The 2-His-1-carboxylate facial triad: a versatile platform for dioxygen activation by mononuclear non-heme iron (II) enzymes, JBIC J. Biol. Inorg. Chem. 10 (2005) 87–93.
[14] P.C. Bruijnincx, G. van Koten, R.J.K. Gebbink, Mononuclear non-heme iron enzymes with the 2-His-1-carboxylate facial triad: recent developments in enzymology and modeling studies, Chem. Soc. Rev. 37 (2008) 2716–2744.
[15] E.L. Hegg, The 2-His-1-carboxylate facial triad—an emerging structural motif in mononuclear non-heme iron (II) enzymes, Eur. J. Biochem. 250 (1997) 625–629.
[16] N.D. Das, K.H. Jung, Y.G. Chai, The role of NF-κB and H3K27me3 demethylase, Jmjd3, on the anthrax lethal toxin tolerance of RAW 264.7 cells, PLoS One 5 (2010) e9913.
[17] A. Salminen, K. Kaarniranta, M. Hiltunen, A. Kauppinen, Histone demethylase Jumonji D3 (JMJD3/KDM6B) at the nexus of epigenetic regulation of inflammation and the aging process, J. Mol. Med. 92 (2014) 1035–1043.
[18] J. Anderton, S. Bose, M. Vockerodt, K. Vrzalikova, W. Wei, M. Kuo, et al., The H3K27me3 demethylase, KDM6B, is induced by Epstein–Barr virus and over-expressed in Hodgkin's Lymphoma, Oncogene 30 (2011) 2037–2043.
[19] K. Agger, P.A. Cloos, L. Rudkjær, K. Williams, G. Andersen, J. Christensen, et al., The H3K27me3 demethylase JMJD3 contributes to the activation of the INK4A–ARF locus in response to oncogene-and stress-induced senescence, Genes Dev. 23 (2009) 1171–1176.
[20] M. Barradas, E. Anderton, J.C. Acosta, S. Li, A. Banito, M. Rodriguez-Niedenführ, et al., Histone demethylase JMJD3 contributes to epigenetic control of INK4a/ARF by oncogenic RAS, Genes Dev. 23 (2009) 1177–1182.
[21] F. De Santa, V. Narang, Z.H. Yap, B.K. Tusi, T. Burgold, L. Austenaa, et al., Jmjd3 contributes to the control of gene expression in LPS-activated macrophages, EMBO J. 28 (2009) 3341–3352.
[22] K.A. Gallagher, A. Joshi, W.F. Carson, M. Schaller, R. Allen, S. Mukerjee, et al., Epigenetic changes in bone marrow progenitor cells influence the

inflammatory phenotype and alter wound healing in type 2 diabetes, Diabetes 64 (2015) 1420–1430.
[23] C. Busch, M. Burkard, C. Leischner, U.M. Lauer, J. Frank, S. Venturelli, Epigenetic activities of flavonoids in the prevention and treatment of cancer, Clin. Epigenet. 7 (2015) 1.
[24] T.E. McAllister, K.S. England, R.J. Hopkinson, P.E. Brennan, A. Kawamura, C.J. Schofield, Recent progress in histone demethylase inhibitors, J. Med. Chem. 59 (2016) 1308–1329.
[25] N.R. Rose, M.A. McDonough, O.N. King, A. Kawamura, C.J. Schofield, Inhibition of 2-oxoglutarate dependent oxygenases, Chem. Soc. Rev. 40 (2011) 4364–4397.
[26] I.F. Cheng, K. Breen, On the ability of four flavonoids, baicilein, luteolin, naringenin, and quercetin, to suppress the Fenton reaction of the iron-ATP complex, Biometals 13 (2000) 77–83.
[27] K.E. Heim, A.R. Tagliaferro, D.J. Bobilya, Flavonoid antioxidants: chemistry, metabolism and structure-activity relationships, J. Nutr. Biochem. 13 (2002) 572–584.
[28] M. Sakurai, N.R. Rose, L. Schultz, A.M. Quinn, A. Jadhav, S.S. Ng, et al., A miniaturized screen for inhibitors of Jumonji histone demethylases, Mol. BioSyst. 6 (2010) 357–364.
[29] B.Y. Kang, S.H. Kim, D. Cho, T.S. Kim, Inhibition of interleukin-12 production in mouse macrophagesvia decreased nuclear factor-κB DNA binding activity by myricetin, a naturally occurring flavonoid, Arch. Pharm. Res. 28 (2005) 274–279.
[30] D.K. Semwal, R.B. Semwal, S. Combrinck, A. Viljoen, Myricetin: a dietary molecule with diverse biological activities, Nutrients 8 (2016) 90.
[31] S.-Y. Ko, Myricetin suppresses LPS-induced MMP expression in human gingival fibroblasts and inhibits osteoclastogenesis by downregulating NFATc1 in RANKL-induced RAW 264. 7 cells, Arch. Oral Biol. 57 (2012) 1623–1632.
[32] Schrödinger Release 2016-2: Maestro, v., Schrödinger, LLC, New York, NY, 2016.
[33] H. Berman, J. Westbrook, Z. Feng, G. Gilliland, T. Bhat, H. Weissig, et al., The Protein Data Bank, Nucleic Acids Res. 28 (2016) 235–242, View Article PubMed/NCBI Google Scholar. 2000.
[34] P.W. Rose, A. Prlić, C. Bi, W.F. Bluhm, C.H. Christie, S. Dutta, et al., The RCSB Protein Data Bank: views of structural biology for basic and applied research and education, Nucleic Acids Res. 43 (2015) D345–D356.
[35] T. Sterling, J.J. Irwin, ZINC 15—ligand discovery for everyone, J. Chem. Inf. Model. 55 (11) (2015).
[36] J.J. Irwin, T. Sterling, M.M. Mysinger, E.S. Bolstad, R.G. Coleman, ZINC: a free tool to discover chemistry for biology, J. Chem. Inf. Model. 52 (2012) 1757–1768.
[37] Schrödinger Release 2016-2: LigPrep, v., Schrödinger, LLC, New York, NY, 2016.
[38] D. Shivakumar, J. Williams, Y. Wu, W. Damm, J. Shelley, W. Sherman, Prediction of absolute solvation free energies using molecular dynamics free energy perturbation and the OPLS force field, J. Chem. Theory Comput. 6 (2010) 1509–1519.
[39] G.M. Sastry, M. Adzhigirey, T. Day, R. Annabhimoju, W. Sherman, Protein and ligand preparation: parameters, protocols, and influence on virtual screening enrichments, J. Comput. Aided Mol. Des. 27 (2013) 221–234.
[40] Schrödinger Release 2016-2: Schrödinger Suite 2016-2 Protein Preparation Wizard; Epik version 3.6, S., LLC, New York, NY, 2016; Impact version 7.1, Schrödinger, LLC, New York, NY, 2016; Prime version 4.4, Schrödinger, LLC, New York, NY, 2016.
[41] M.P. Jacobson, D.L. Pincus, C.S. Rapp, T.J. Day, B. Honig, D.E. Shaw, et al., A hierarchical approach to all-atom protein loop prediction, Proteins Struct. Funct. Bioinf. 55 (2004) 351–367.
[42] R.A. Friesner, R.B. Murphy, M.P. Repasky, L.L. Frye, J.R. Greenwood, T.A. Halgren, et al., Extra precision glide: docking and scoring incorporating a model of hydrophobic enclosure for protein-ligand complexes, J. Med. Chem. 49 (2006) 6177–6196.
[43] R.A. Friesner, J.L. Banks, R.B. Murphy, T.A. Halgren, J.J. Klicic, D.T. Mainz, et al., Glide: a new approach for rapid, accurate docking and scoring. 1. Method and assessment of docking accuracy, J. Med. Chem. 47 (2004) 1739–1749.
[44] Small-Molecule Drug Discovery Suite 2016-2: Glide, v., Schrödinger, LLC, New York, NY, 2016.
[45] Schrödinger Suite 2009 Induced Fit Docking protocol; Glide version 5.5, S., LLC, New York, NY, 2009; Prime version 2.1, Schrödinger, LLC, New York, NY, 2009.
[46] S. Genheden, U. Ryde, The MM/PBSA and MM/GBSA methods to estimate ligand-binding affinities, Expert Opin. Drug Discov. 10 (2015) 449–461.
[47] J. Li, R. Abel, K. Zhu, Y. Cao, S. Zhao, R.A. Friesner, The VSGB 2. 0 model: a next generation energy model for high resolution protein structure modeling, Proteins Struct. Funct. Bioinf. 79 (2011) 2794–2812.
[48] QikProp, v., Schrödinger, LLC, New York, NY, 2012.